East Eur. J. Phys. **2**. 135-145 (2021) DOI:10.26565/2312-4334-2021-2-11

PACS: 41.20.Cv; 61.43.Bn; *68.55.ag*; *68.55.jd*; 73.25.+i; 72.80.Tm; 74.62.Dh; 78.20.Bh; 89.30.Cc

NUMERICAL MODELING AND ANALYSIS OF HTM-FREE HETEROJUNCTION SOLAR CELL USING SCAPS-1D

Eli Danladi[a,*], Alhassan Shuaibu[b], Muhammad Sani Ahmad[b], Jamila Tasiu[b]
[a]*Department of Physical Sciences, Greenfield University, Kaduna, Nigeria*
[b]*Department of Physics, Kaduna State University, Kaduna, Nigeria*
**Coresponding Author: danladielibako@gmail.com, +2348063307256*
Received January 19, 2021; revised March 27, 2021; accepted April 10, 2021

In this research paper, a HTM-free perovskite solar cell (PSC) structure with Titanium (TiO_2), methyl ammonium lead triiodide ($CH_3NH_3PbI_3$) and platinum (pt) as electron transport material (ETM), photon harvester and metal back contact is proposed. Solar Cell Capacitance Simulator (SCAPS-1D) program was used to implement the model and simulation. Effect of parameters such as thickness of ETM, thickness of absorber, doping concentration of ETM & absorber and electron affinity (EA) of ETM were investigated systematically. From the obtained results, it was found that the parameters affect the performance of the solar cell. When the thickness of ETM was varied from 0.02 to 0.10 μm . The results show that photovoltaic parameters decrease with the thickness increase. When the thickness of the absorber was varied from 0.1 to 1.0 μm , the optimized value was found at thickness of 0.4 μm . When the doping concentration of absorber and EMT were varied from 10^{10}–10^{17} cm^{-3} and from 10^{15}–10^{20} cm^{-3}, the highest values of PCEs were obtained at 10^{16} cm^{-3} and 10^{20} cm^{-3} for Absorber and ETM. Also when the EA was varied in the range of 3.7 eV to 4.5 eV, the optimized value was at 3.7 eV. Upon optimization of the above mentioned parameters, power conversion efficiency (PCE) was found to be 25.75 %, short circuit current density (J_{sc}) 23.25 $mAcm^{-2}$, open circuit voltage (V_{oc}) 1.24 V and fill factor (FF) 89.50 %. The optimized result shows an improvement of ~1.95 times in PCE, ~1.06 times in J_{sc}, ~1.44 times in V_{oc} and ~1.28 times in FF as compared to the initial device with the following parameters, PCE=13.22 %, J_{sc}=21.96 $mAcm^{-2}$, V_{oc}=0.86 V and FF=69.94 %.
KEYWORDS: perovskite solar cells, HTM free, device modeling, simulation, band gap offset

Recently, organic-inorganic metal halide perovskite solar cells have taken the renewable energy community by storm and subsequently gained attention of several world's researchers due to its high performance and low cost. Several advantages of perovskite absorber have made it a choice of candidate for application photovoltaic structures, among which include, tuned band gap, small exciton energy, excellent bipolar carrier transport, long electron-hole diffusion, and amazingly high tolerance to defects [1-7]. The properties exhibited by this material in solar cells results to enhanced power conversion efficiency from 3.9 % [8] to over 25 % [9]. However, some draw backs such as instability, electron transport resistance between TiO_2 and perovskite absorber and the use of costly hole transport material (HTM) (such as spiro-Omeotad) has prevented its outdoor usage. Therefore, the use of readily available and stable materials having high hole mobility with simple route of synthesis is desirable [10-12].

A report on perovskite solar cell without HTM was demonstrated firstly by Etgar et al. [13], where the perovskite absorber functions as a transporter of hole and harvester of photon energy simultaneously and results to a PCE of 5%. The results demonstrate simplicity and high reduction in cost of fabrication and a relatively improved stability as a result of HTM elimination. Also, in 2014, Li et al. [14] followed the same route by replacing metal back contact with laminated carbon nanotubes (CNTs) to collect holes from absorber and block electrons from ETM and results to a PCE of 6.87%. Eli et al. [9] developed a PSC without HTM with elcocarb as metal back contact to collect hole and realized a PCE of 3.80 %.

Recently a PCE of 10.95% with about 95% stability of their initial efficiency after being exposed to air (relative humidity of 25-35%) for 20 days, was demonstrated by Zhang et al [15]. In a simulation studies by Lin et al [16], a PCE of 15.02% was obtained with a structure without HTM and ZnO as ETM. Theoretical studies carried out by Wang and group [17] shows that the careful selection of thickness of the absorber and p-type doping were crucial to the PCE of the HTM-free PSCs.

The HTM-free PSC is a simple and promising way to realize good PCE but some factors deter its practical use. PSC devices mostly make use of costly gold (Au) as a back contact. The Au metal contact is not only expensive but the process of synthesis and development require the use of high-technology (such as high-vacuum evaporation technique). Platinum metal, with the work function of 5.93 [18], has been applied in perovskite solar cells with HTM and without HTM, but the PV parameters were of poor values for HTM (Jsc=7.17 $mAcm^{-2}$, Voc=0.69, FF=62.62 and PCE=3.08 %). And for the device without HTM, the PV parameters are Jsc=20.58 $mAcm^{-2}$, Voc=1.006, FF=71.07 and PCE=14.72 %.

To realize higher photovoltaic parameters and proper optimized architecture in HTM-free PSC, systematic understanding of the operational mechanism needs to be uncovered. Yet till now, numerical modeling and simulation of the HTM-free PSCs with platinum metal contact and TiO_2 ETM has seldom been reported. Platinum metal has a high work function and good chemical stability. In view of that, this research paper, attempts to present a detailed numerical modeling and simulation of HTM-free PSCs based on solar cell capacitance simulator (SCAPS) software to systematically study the influence of some material (such as thickness of ETM, thickness of absorber layer, doping concentration of

ETM, doping concentration of absorber layer, electron affinity of ETM etc), with the goal of uncovering the hidden mechanism for PCE improvement.

METHOD AND METHODOLOGY

The nature of the defect is set as Gaussian and defect density is set as 1×10^{18} cm^{-3} [19,20]. Table 1 shows the defect parameters which are used in the simulation. Basic parameters for each material used in the simulation are summarized in Table 2. Thermal velocities of hole and electron are selected as 10^7 cms^{-1} [19-22]. The optical reflectance is considered to be zero at the surface and at each interface [19]. Parameters are optimized in the study by using control variable method. The initial total defect density of the absorber layer is assumed to be 2.5×10^{13} cm^{-3}. Neutral Gaussian distribution defect is selected in the absorber layer and characteristic energy is set to be 0.1 eV [19]. One defect interface is inserted for carrier recombination. The interface defect layer (IDL) is introduced in the $TiO_2/CH_3NH_3PbI_3$ interface to investigate the influence of interfacial recombination on the photovoltaic performance. The work functions of the front contact and back contact are 4.40 eV and 5.93 eV respectively [18,23]. A working temperature of 300K, solar spectrum AM1.5 and a Scanning voltage of 0-1.3 V were used for all simulations.

Table 1. Defect parameters of interfaces and absorber [19,20,23]

Parameters	$CH_3NH_3PbI_3$	$TiO_2/CH_3NH_3PbI_3$ interface
Defect type	Neutral	Neutral
Capture cross section for electrons (cm^2)	2×10^{-14}	2×10^{-14}
Capture cross section for holes (cm^2)	2×10^{-14}	2×10^{-14}
Energetic distribution	Gaussian	Single
Energy level with respect to Ev (eV)	0.500	0.650
Characteristic energy (eV)	0.1	0.1
Total density (cm^{-3})	1×10^{15}–1×10^{19}	1×10^{17}

Table 2. Simulation parameters of PSCs devices [19, 20,23,24]

Parameters	**FTO**	**ETM (TiO_2)**	**Absorber**
Thickness (μm)	0.4	0.05	0.45
Band gap energy Eg (eV)	3.5	3.26	1.55
Electron affinity χ (eV)	4.0	4.2	3.90
Relative permittivity *er*	9	10	6.50
Effective conduction band density Nc (cm^{-3})	2.2×10^{18}	2.2×10^{28}	2.2×10^{18}
Effective valance band density Nv (cm^{-3})	2.2×10^{18}	2.2×10^{18}	2.2×10^{18}
Electron mobility μn (cm^2 V^{-1} s^{-1})	20	20	2
Hole mobility μp (cm^2 V^{-1} s^{-1})	10	10	2
Donor concentration N_D (cm^{-3})	1×10^{19}	1×10^{17}	0
Acceptor concentration N_A (cm^{-3})	0	0	1×10^{13}
Defect density N_t (cm^{-3})	1×10^{15}	1×10^{15}	2.5×10^{13}

RESULTS AND DISCUSSION

Structure of PSC in the simulation and Energy level diagram of HTM free PSC device

The modeled PSC and band structure of the HTM free perovskite solar cell obtained with simulated parameters in Tables 1 and 2 are illustrated in Figure 1 (a) and (b). The interface conduction and valence band offset at the $TiO_2/CH_3NH_3PbI_3$ interface are ΔEc=0.31 eV and ΔEv=2.02 eV as shown in Figure 1(b).

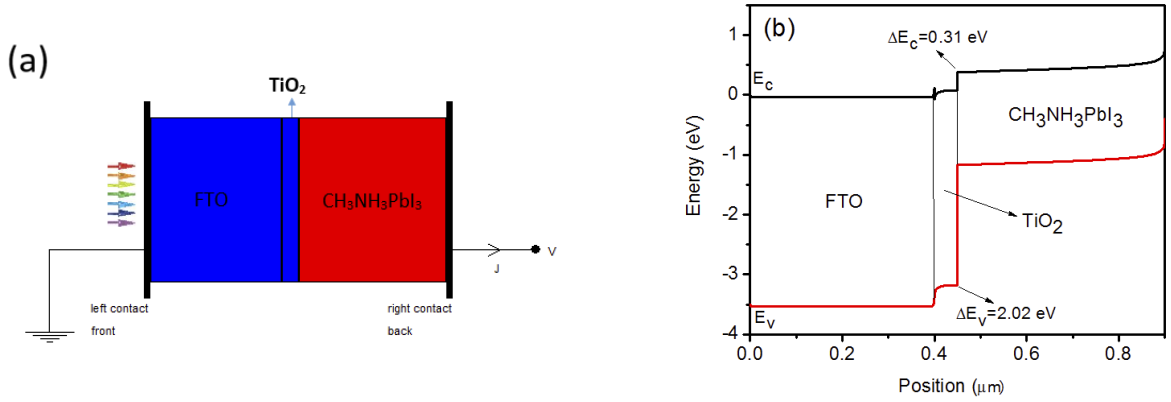

Figure 1. (a) The structure of perovskite solar cell in the simulation and (b) Energy band diagram of $TiO_2/CH_3NH_3PbI_3$ PSC device.

The value of ΔEc prevents the flow of electron charge carrier from the electron transport layer to perovskite layer to the pt metal contact so as to avoid quenching in the perovskite layer. While the large value of ΔEv denies the flow of holes to the platinum-back contact to prevent their recombination with the electrons in the perovskite layer. These values

can be seen important as they encouraged collection of charge carriers which results to higher photovoltaic performance in PSCs. As such, from the result of the band gap structure, TiO_2 and $CH_3NH_3PbI_3$ can form a p-n junction when combined together to be applied in photovoltaics.

Performance parameters from initial simulation

The J-V characteristics of the reference modeled PSC device under illumination and in the dark is shown in figure 2(a). Under illumination, a J_{sc} of 21.96 $mAcm^{-2}$, Voc of 0.86 V, FF of 69.94 %, and PCE of 13.22 % are obtained. The V_{oc} simulated in this studies agrees with V_{oc} (0.85 V) in experimental work demonstrated by a group of researchers [9]. However, the values of PCE, FF and J_{sc} are higher than ones obtained from experimental research work, this may be due to the lesser series resistance arising from pt metal contact or FTO and the optical reflectance is considered to be zero at the surface and at each interface during our simulation [25].

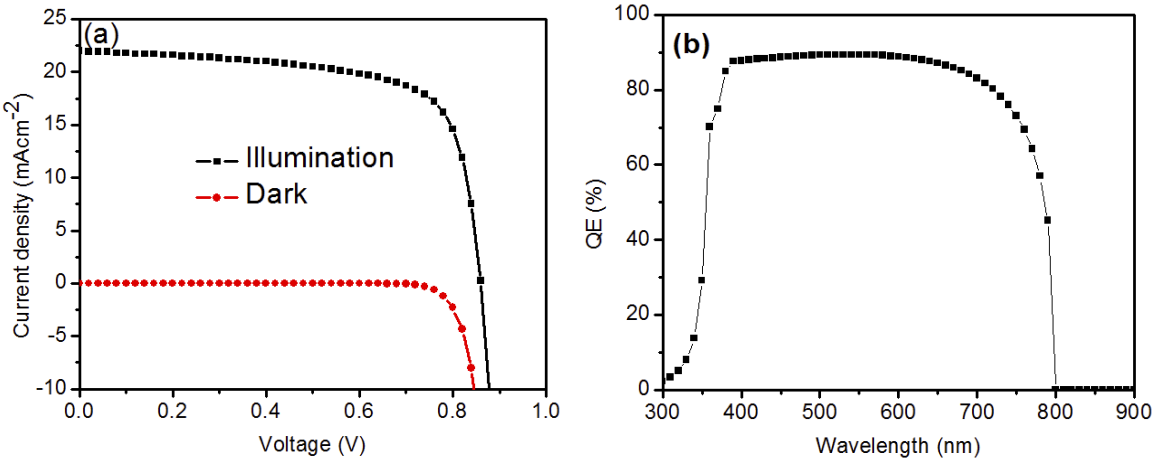

Figure 2. (a) J–V curve of PSC with initial parameters, (b) spectra of the device with initial parameters

As illustrated in Figure 2(a), Under the dark condition, there is no current flowing thereby behaving as a diode resulting to an extreme minimum value of J_{sc} when the voltage is less than the knee voltage (0.6 V) and decreases gradually when the voltage further increases [25]. This results to rectifying characteristics and this rectifying behavior is a feature of photovoltaic devices and is a consequence of the asymmetric junction needed to separate charges.
In the quantum efficiency (QE) of the device shown in figure 2 (b) which is within the wavelength of 300 nm and 900 nm has maximum attained value of 90 % at 550 nm. Optical absorption edge is red shifted to 800 nm which corresponds to a band gap of 1.55 eV in $CH_3NH_3PbI_3$. The QE sweeps across the whole visible spectrum which to an extent agrees with experimental work [9].

Effect of thickness of Electron transport layer

Figures 3(a), (b) and (c) show the J-V behavior, QE and the plot of solar cell parameters; V_{OC}, J_{SC}, FF and PCE versus thickness of the ETM. Thickness of ETM was varied from 0.02 to 0.10 μ m. The results show that both the PCE, Jsc, Voc and FF decrease with the thickness of ETM. The slight decrease in the photovoltaic properties is due to fractional absorption of incident light by the TiO_2 layer and the bulk/surface recombination at the interface which result to lesser electron and hole pairs extraction [26]. The decrease in FF is connected to the increase in series resistance.

Figure 3(b) displays the QE of the perovskite solar cell as a function of wavelength within the range of 300-900 nm with varied ETM layer thickness. It can be seen that the QE reaches a maximum value in the wavelength range of 380−570 nm and gradually decreases at longer wavelengths until 800 nm, which corresponds to its absorption spectrum demonstrated in figure 3(b). Table 3 shows the photovoltaic parameters obtained during the simulation.

Table 3. J-V characteristic parameters with the variation of thickness of ETM

Parameters T (μ m)	J_{sc} (mAcm^{-2})	V_{oc} (V)	*FF*	PCE (%)
0.02	22.05	0.88	70.17	13.63
0.03	22.01	0.87	70.11	13.40
0.04	21.98	0.86	69.96	13.28
0.05	21.96	0.86	69.94	13.22
0.06	21.94	0.86	69.91	13.18
0.07	21.93	0.86	69.91	13.17
0.08	21.92	0.86	69.91	13.15
0.09	21.90	0.86	69.91	13.15
0.10	21.89	0.86	69.92	13.14

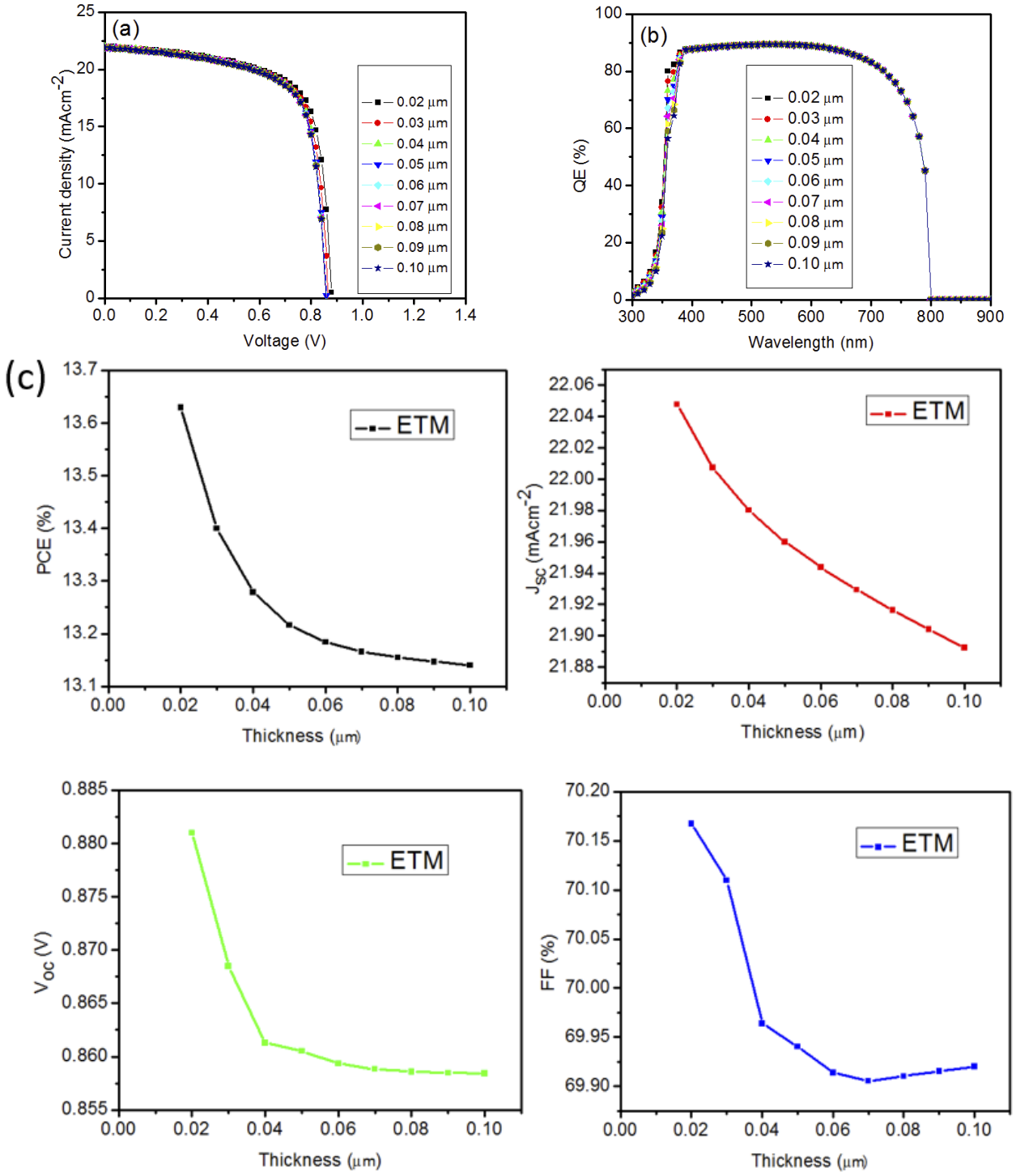

Figure 3. (a) J–V curves of PSC with different values of thickness of ETM, (b) QE with different values of thickness of ETM, (c) Variation in performance parameters of PSC with thickness of ETM.

Effect of thickness of absorber layer

The influence of thickness of absorber on the solar cell parameters; V_{OC}, J_{SC}, FF and PCE is shown in figure 4 (a). The J-V and QE of the varied absorber thickness is shown in Figure 4 (a) and (b).

As shown in Figure 4 (a), Jsc increases from 12.33 to 22.36 mAcm^{-2} with thickness increase from 0.1 to 0.6 which is due to the increase in carrier generation and dissociation, then starts decreasing from 0.7 to 1.0 μ m which is attributed to high recombination rate within the range of the thickness. FF decreases slightly with thickness increase in the perovskite layer. Table 4 shows the photovoltaic parameters obtained during the simulation. The PCE increase with increase in layer thickness from 0.1 to 0.4 μ m due to the production of new charge carriers. However, PCE decreases from thickness of 0.5 to 1.0 μ m due to lesser electron and hole pairs extraction rate that leads to recombination process [27].

Figure 4 (c) exhibits the spectral response of the PSCs as a function of wavelength with varied $CH_3NH_3PbI_3$ layer thickness within range of 300 to 900 nm. The QE first increases rapidly with the $CH_3NH_3PbI_3$ thickness increasing from 0.1 to 0.4 μ m, and the QE increase slightly after the thickness is greater than 0.4 μ m, which shows that 0.4 μ m thickness of $CH_3NH_3PbI_3$ layer can absorb most of the incident photons and the part beyond 0.4 μ m can only contribute little to the PSC performance. Therefore, the optimized perovskite absorber layer thickness is around 0.4 μ m which gives V_{OC} of 0.86 V, J_{SC} of 21.63 mAcm^{-2}, FF of 71.39 % and PCE of 13.21 %.

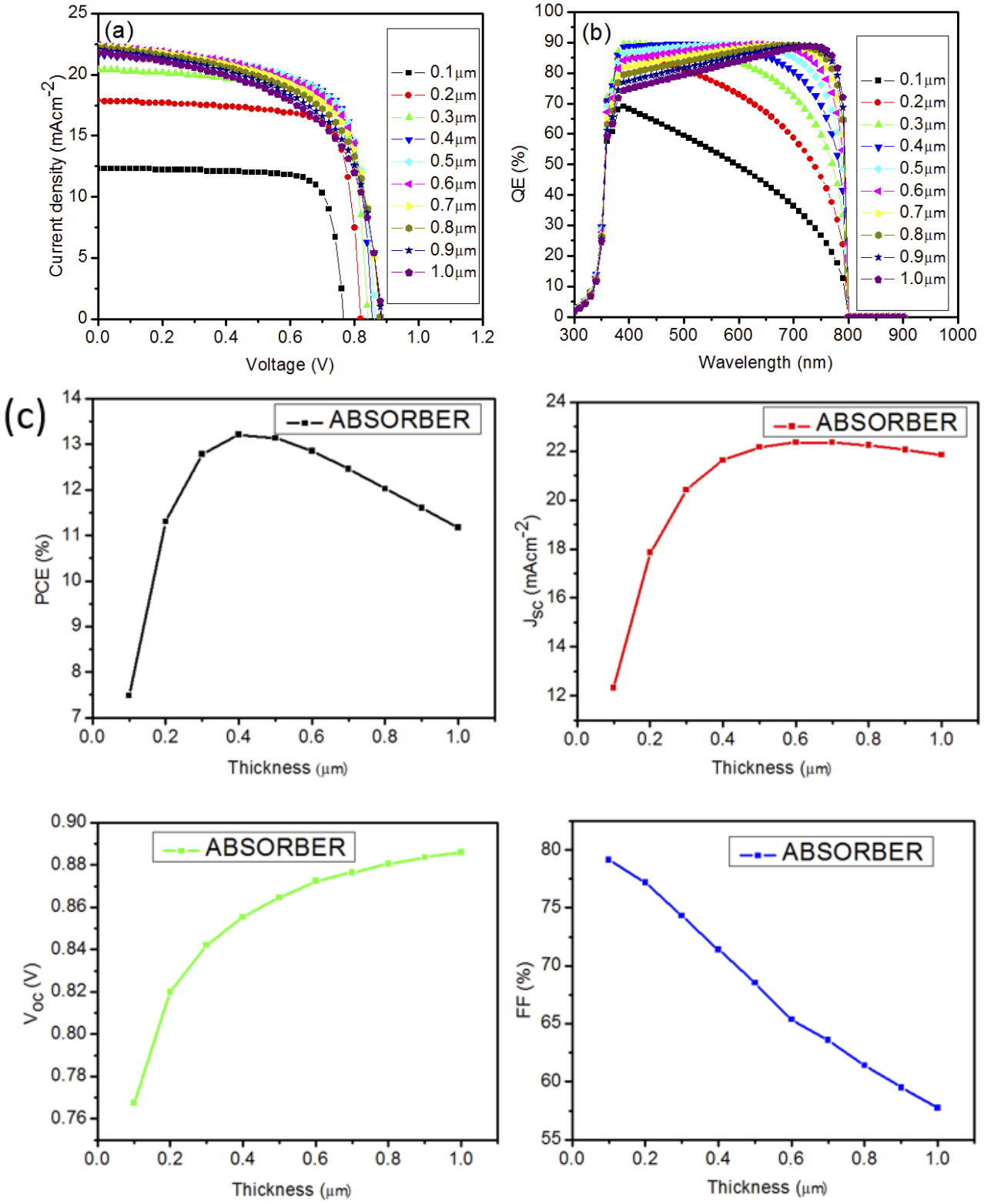

Figure 4. (a) J–V curves of PSC with different values of thickness of absorber layer, (b) QE with different values of thickness of absorber layer, (c) Variation in performance parameters of PSC with thickness of absorber layer

Table 4. J-V characteristic parameters with the variation of thickness of absorber

Parameters T (μ m)	J_{sc} (mAcm^{-2})	V_{oc} (V)	*FF*	PCE (%)
0.1	12.34	0.77	79.12	7.48
0.2	17.85	0.82	77.16	11.30
0.3	20.42	0.84	74.32	12.78
0.4	21.63	0.86	71.39	13.21
0.5	22.17	0.86	68.54	13.13
0.6	22.36	0.87	65.36	12.85
0.7	22.36	0.88	63.59	12.46
0.8	22.24	0.88	61.39	12.02
0.9	22.06	0.88	59.50	11.60
1.0	21.85	0.89	57.73	11.18

Effect of doping concentration (N_A) of absorber layer

Doping is the process of introducing impurities in absorber layer. The effect of doping concentration on the performance of perovskite solar cell is studied by choosing the values of N_A in the range of 10^{10}–10^{17} cm^{-3} while keeping N_D for ETM at 10^{17} cm^{-3}. Table 5 gives the performance parameters of PSCs with various values of doping concentration. The highest value of PCE was obtained with doping concentration of 10^{16} cm^{-3} which shows value of 14.89 %. The highest value of fill factor was also observed at the same N_A. The PCE and the FF remained constant with increase in doping concentration from 10^{10}–10^{13} cm^{-3} and increases with doping concentration from 10^{13}–10^{16} cm^{-3}. Beyond the values, a decrease in PCE and FF was noticed. The obtained results show that charge carriers are transported and collected optimally at the same irradiance when N_A of the $CH_3NH_3PbI_3$ is 1×10^{16} cm^{-3}. The J_{sc} and Voc remained constant with increasing N_A from 10^{10}-10^{13} cm^{-3}, while beyond 10^{13} cm^{-3}, J_{sc} increases with increasing N_A and V_{oc} decreases with increasing N_A. The ability of the photo-generated carriers is weak, resulting to a reduced Voc which caused a full depletion and strong electric field in the absorber layer.

The QE with respect to wavelength is as shown in Figure 5(b) with varied concentration from 10^{10}-10^{16} cm^{-3}. It can be seen that the QE rapidly increase within the wavelength range of 300 – 380 nm and thereby maintained a constant until at 630 nm before it decreases rapidly to 800 nm from 10^{10}-10^{15} cm^{-3}. From 10^{15}-10^{13} cm^{-3} a gradual decrease from the cutout of 390 nm until 800 nm was observed. The result shows that the solar cell functions effectively within the visible region.

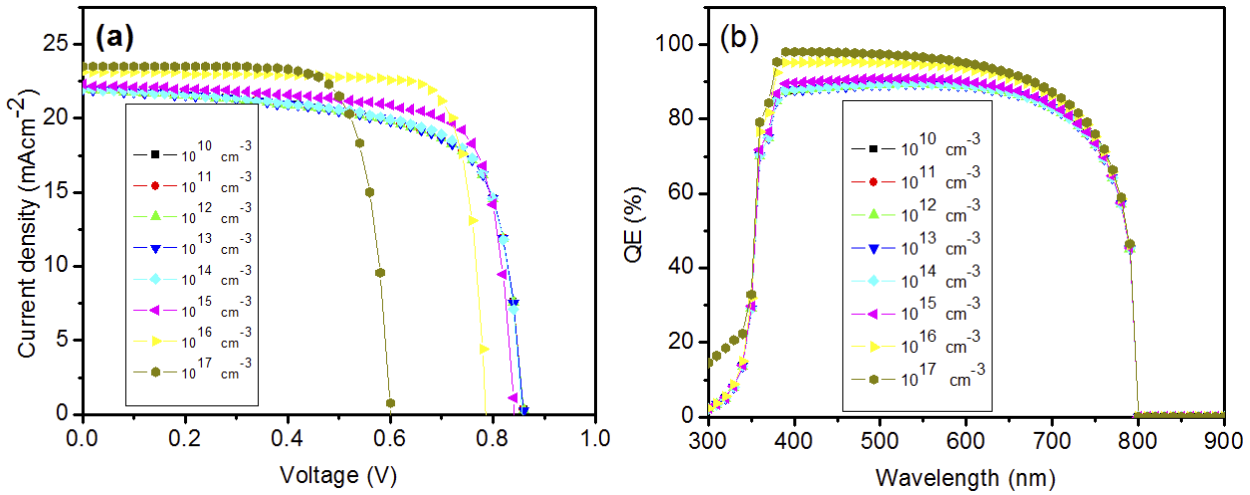

Figure 5. (a) J–V curves of PSC with different values of doping concentration in absorber layer, (b) QE with different values of doping concentration in absorber layer

Table 5. Dependence of solar cell performance on the doping concentration of Absorber layer

Parameters N_A(cm^{-3})	J_{sc} (mAcm^{-2})	V_{oc} (V)	*FF*	PCE (%)
1E+10	21.96	0.86	69.86	13.20
1E+11	21.96	0.86	69.86	13.20
1E+12	21.96	0.86	69.87	13.20
1E+13	21.96	0.86	69.94	13.22
1E+14	22.00	0.86	70.65	13.34
1E+15	22.27	0.84	75.67	14.19
1E+16	23.13	0.79	81.85	14.89
1E+17	23.54	0.61	76.12	10.77

Effect of doping concentration (N_D) of ETM

The effect of doping concentration on the performance of perovskite solar cells is examined by varying the values of N_D in the range of 10^{15}–10^{20} cm^{-3} while keeping N_A for absorber at 10^{13} cm^{-3}. Figure 6 (a) and (b) shows the J–V curves of PSC with different values of doping concentration in ETM and QE with different values of doping concentration in ETM layer. When the doping concentration is varied from 10^{15}–10^{20} cm^{-3}, it was depicted from Table 6 that, the PCE increased from 12.52 % to 16.62 %. The increase in PCE is as a result of reduction in series resistance due to increase in optical conductivity of the ETM. Hence, the doping concentration N_D is set at 10^{20} cm^{-3}. Similarly, there was increase in other photovoltaic parameters (J_{sc}, V_{oc} and FF) with increase in doping concentration values. The optimized values of the performance parameters are PCE=16.62 %, Jsc=22.24 $mAcm^{-2}$, Voc=1.04 V and FF=72.18%.

The increase in the photovoltaic parameters with increasing N_D could be explained as follows: Auger recombination rate decreases with doping density below 10^{20} cm^{-3}. It is seen that the quenching losses decreases when N_D is below 10^{20} cm^{-3}. We therefore speculate that, optimum doping concentration of ETM enhances the Voc and Jsc which subsequently results to higher PCE.

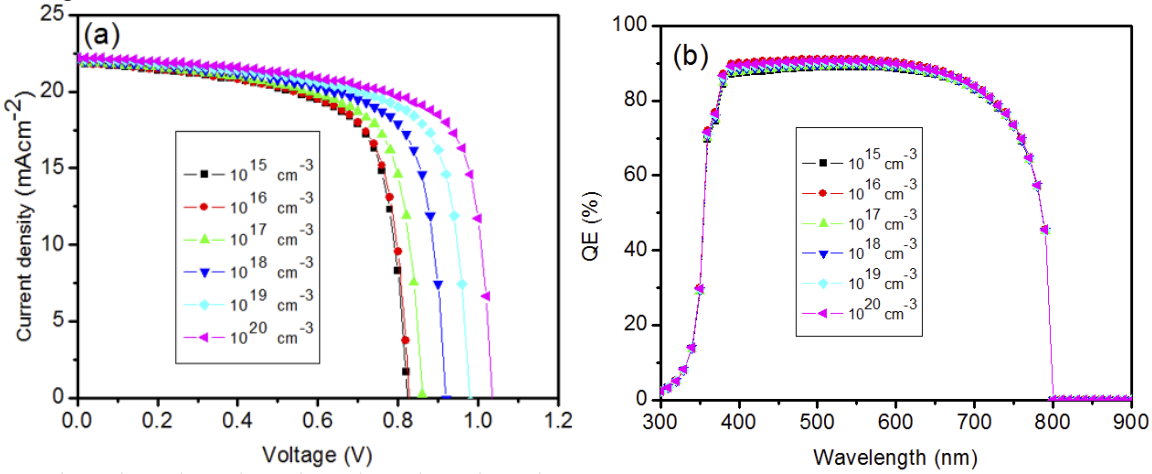

Figure 6. (a) the J–V curves of PSC with different values of doping concentration in ETM, (b) QE with different values of doping concentration in ETM layer

Table 6. Dependence of solar cell performance on the doping concentration of ETM

Parameters N_A(cm^{-3})	J_{sc} ($mAcm^{-2}$)	V_{oc} (V)	*FF*	PCE (%)
1E+15	21.87	0.82	69.51	12.52
1E+16	21.89	0.83	69.59	12.62
1E+17	21.96	0.86	69.94	13.22
1E+18	22.07	0.92	70.59	14.33
1E+19	22.16	0.98	71.20	15.45
1E+20	22.24	1.04	72.18	16.62

Influence of electron affinity of ETM

The effect of electron affinity (EA) on the performance of perovskite solar cell is examined by varying the values of EA in the range of 3.7 eV to 4.5 eV. Figure 7 (a), (b) and (c) shows the J–V curves of PSC with different values of EA of ETM, QE with different values of EA of ETM layer and Photovoltaic parameters with respect to EA.

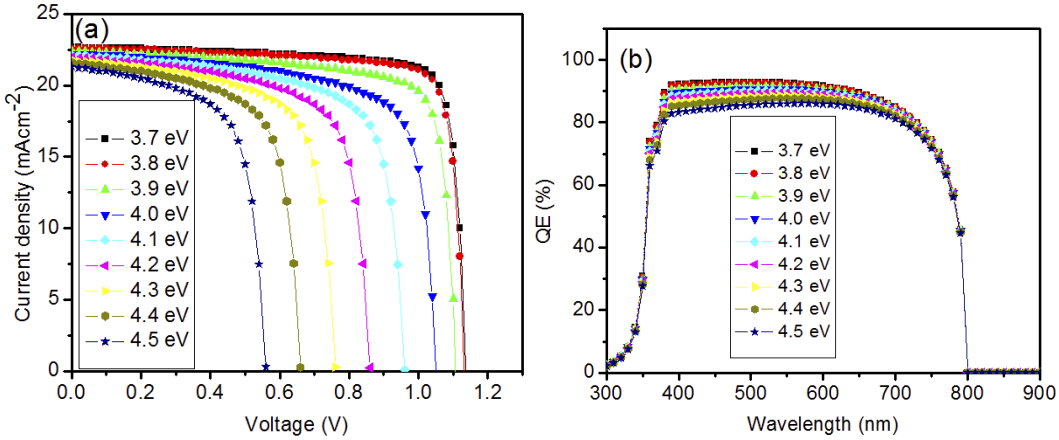

Figure 7. (a) J–V curves of PSC with different values of EA of ETM, (b) QE with different values of EA of ETM, (c) Variation in performance parameters of PSC with EA of ETM (*continued on the next page*)

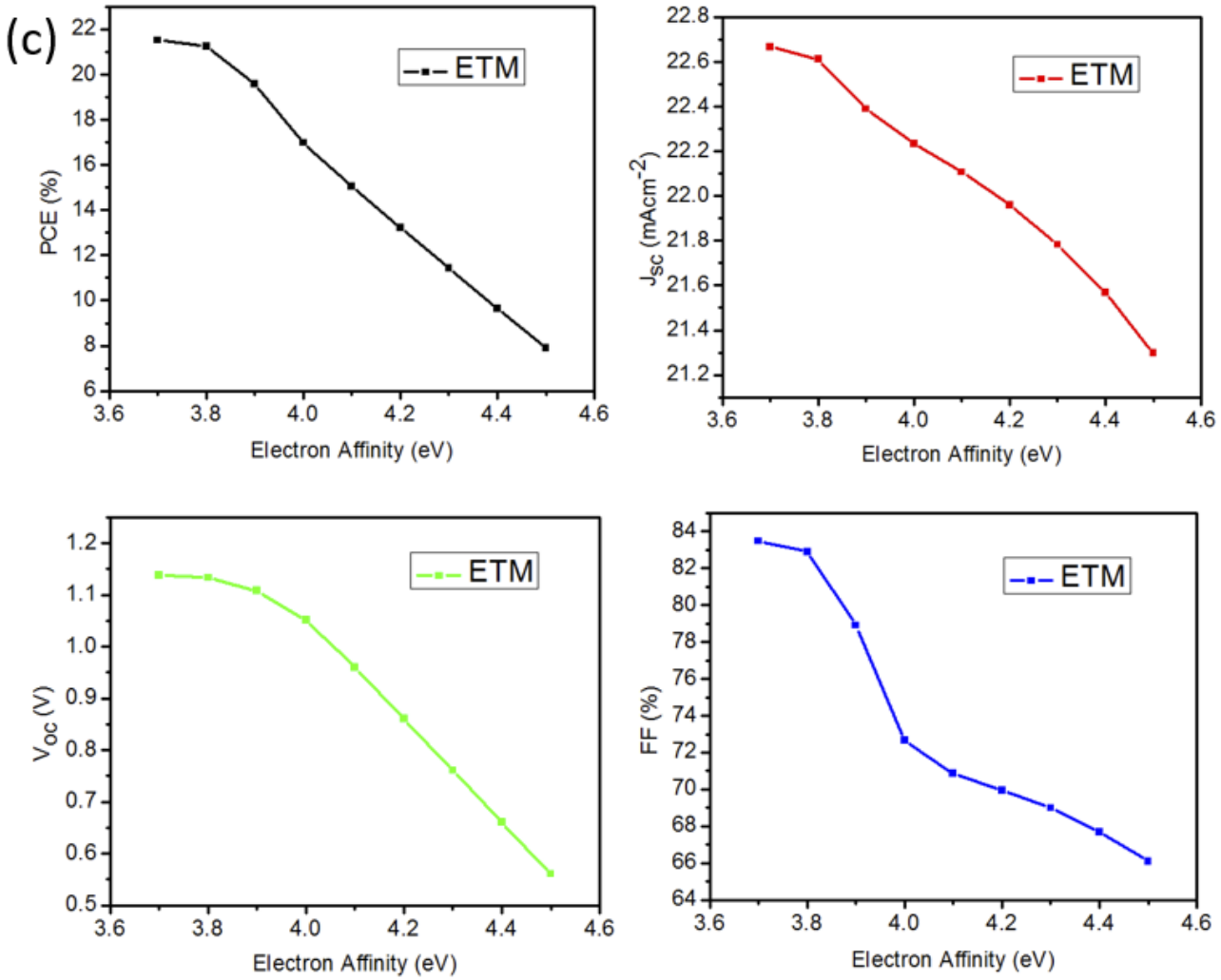

Figure 7. (a) J–V curves of PSC with different values of EA of ETM, (b) QE with different values of EA of ETM, (c) Variation in performance parameters of PSC with EA of ETM

Figures 7(c) shows variation of PCE, Voc, Jsc and FF with electron affinity of ETM and figure 7(a) show the J-V curve with different electron affinity values. The optimum photovoltaic performance was obtained at EA value of 3.7 eV, which gave PCE, Jsc, Voc and FF as shown in Table 7. It is now evident from our findings that proper selection ETM with good EA can reduce quenching losses in PSCs. Table 7 gives the performance parameters of PSCs with various values of EA.

Table 7. Dependence of solar cell performance on the electron affinity of ETM

Parameters EA (eV)	J_{sc} (mAcm^{-2})	V_{oc} (V)	*FF*	PCE (%)
3.7	22.67	1.14	83.49	21.53
3.8	22.61	1.13	82.90	21.24
3.9	22.39	1.11	78.90	19.58
4.0	22.23	1.05	72.65	16.98
4.1	22.10	0.96	70.86	15.04
4.2	21.96	0.86	69.94	13.22
4.3	21.78	0.76	69.00	11.43
4.4	21.57	0.66	67.69	9.64
4.5	21.30	0.56	66.10	7.89

Performance of PSC with Optimized parameters

After simulating the PSC, the ETM thickness, absorber thickness, doping concentration of absorber and ETM were optimized and the values are as shown in Table 8(a). The final optimized PSC gave a PCE of 25.75 %, Jsc of 23.25 mAcm^{-2}, Voc of 1.24 V and FF of 89.50 %. When the optimized result is compared with the reference initial device, an improvement of ~1.95 times in PCE, ~1.06 times in Jsc, ~1.44 times in Voc and ~1.28 times in FF is obtained over the

device that was not optimized. The behaviour of the JV curve in the dark and under illumination is as shown in figure 8(a). Experimental work of HTM free PSC published by other researchers are compared with the simulated results and summarized in Table 8(b).

In the experimental works, PCEs of 3.80 and 4.2 % were achieved for HTM free PSCs with TiO_2 as ETM. The photovoltaic parameters could be improved further to realize the high photovoltaic values achieved in the simulation. This could be realized by improving the film quality of both the absorber and ETM and also consider proper doping of the absorber and ETM in order to realize good electron density.

The energy diagram of the optimized device is as shown in figure 8(c). From the band structure, the conduction and valence band offset at the $TiO_2/CH_3NH_3PbI_3$ interface were reduced to 0.06 eV and 1.98 eV, which can be considered beneficial for the flow of photo-excited charge carriers to the front electrode and back-metal contact in order to avoid their recombination and quenching losses. The quantum efficiency also shows stronger absorber in the visible region as compared to the device without optimization as shown in figure 8(b).

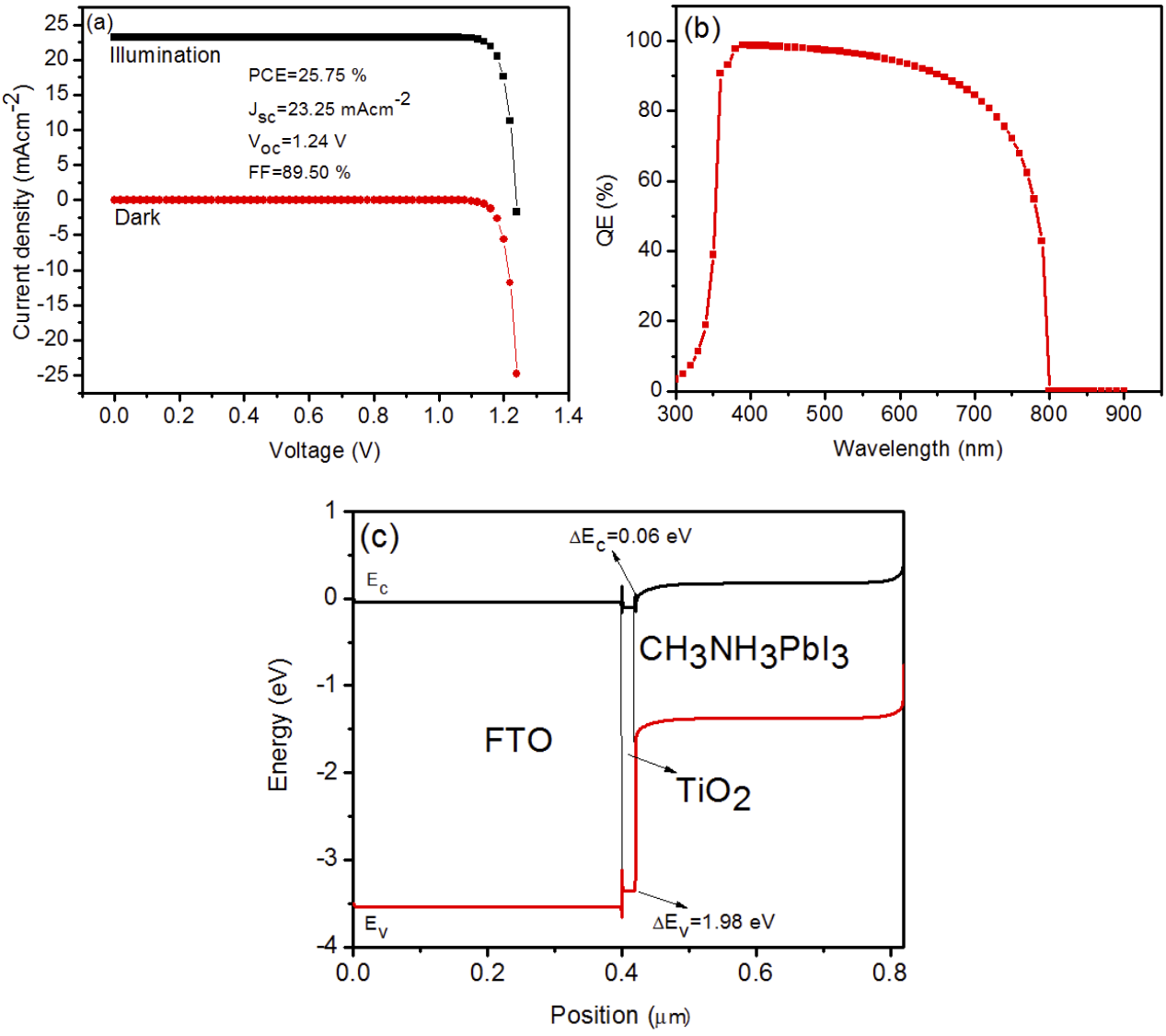

Figure 8. (a) J–V curves of PSC with Optimized parameters, (b) QE with optimized parameters and (c) Energy band diagram of $TiO_2/CH_3NH_3PbI_3$ PSC device

Table 8. (a) Optimized Parameters of the device

Optimized parameters	ETM (TiO2)	Absorber (CH3NH3PbI3)
Thickness (μm)	0.02	0.40
Doping density (N_A) (cm^{-3})	--	1E+16
Doping density (ND) (cm^{-3})	1E+20	--
Electron Affinity (EA)	3.7	--

Table 8(b). Photovoltaic parameters of HTM free perovskite solar cells reported in the experimental work in the literature and simulated results using SCAPS.

Simulation	J_{sc} (mAcm^{-2})	V_{oc} (V)	*FF*	PCE (%)
Initial	21.96	0.86	69.94	13.22
Optimized N_A of absorber	23.13	0.79	81.85	14.89
Optimized N_D of ETM	22.24	1.04	72.18	16.62
Optimized thickness of absorber	21.63	0.86	71.39	13.21
Optimized EA of ETM	22.67	1.14	83.49	21.53
Optimized thickness of ETM	22.05	0.88	70.17	13.63
Final Optimization	23.25	1.24	89.50	25.75
[9]	11.04	0.85	41.00	3.80
[28]	13.60	0.67	45.80	4.20

CONCLUSION

In this work, the HTM free PSC was investigated systematically using Solar Cell Capacitance Simulator (SCAPS-1D) program. The photovoltaic performance of the modeled device with various $CH_3NH_3PbI_3$ thicknesses, ETM thicknesses, ETM electron affinities, ETM doping concentrations and $CH_3NH_3PbI_3$ doping concentrations, has been analyzed. From the obtained results, it is found that the parameters affect the performance of the solar cell. The overall PCE, FF, Jsc, and Voc, of 25.75 %, 89.50 %, 23.25 mAcm^{-2}, and 1.24 V respectively were obtained by using all optimised parameters.

ACKNOWLEDGMENTS

The authors would like to thank Professor Marc Burgelman, Department of Electronics and Information Systems, University of Ghent for the development of the SCAPS software package and for allowing its use.

ORCID IDs

Eli Danladi, https://orcid.org/0000-0001-5109-4690

REFERENCES

[1] J.S. Manser, and P.V. Kamat, Nature Photonics, **8,** 737–747 (2014), https://doi.org/10.1038/nphoton.2014.171.
[2] H. Chen, F. Ye, W. Tang, J. He, M. Yin, Y. Wang, F. Xie, E. Bi, X. Yang, and M. Gratzel, L. Han, Nature, **550,** 92–95 (2017), https://doi.org/10.1038/nature23877.
[3] G. Xing, N. Mathews, S. Sun, S.S. Lim, Y. M. Lam, M. Gratzel, S. Mhaisalkar, and T.C. Sum, Science, **342**, 344–347 (2013), https://doi.org/10.1126/science.1243167.
[4] M. Liu, M. B. Johnston, and H. J. Snaith, Nature, **501**, 395–398 (2013), https://doi.org/10.1038/nature12509.
[5] Z. Wang, Q. Lin, F.P. Chmiel, N. Sakai, L.M. Herz, and H.J. Snaith, Nature Energy, **2,** 17135 (2017), https://doi.org/10.1038/nenergy.2017.135.
[6] Y. Liu, Z. Yang, D. Cui, X. Ren, J. Sun, X. Liu, J. Zhang, Q. Wei, H. Fan, F. Yu, X. Zhang, C. Zhao, and S. Liu, Advanced Materials, **27,** 5176–5183 (2015), https://doi.org/10.1002/adma.201502597.
[7] D. Yang, Z. Yang, W. Qin, Y. Zhang, S. Liu, and C. Li, Journal of Materials Chemistry A, **3,** 9401–9405 (2015), https://doi.org/10.1039/C5TA01824B.
[8] A. Kojima, K. Teshima, Y. Shirai, and T. Miyasaka, Journal of the American Chemical society, **131**(17), 6050-6051 (2009), https://doi.org/10.1021/ja809598r.
[9] D. Eli, M. Y. Onimisi, S. Garba, and J. Tasiu, SN Applied Sciences, **2**, 1769 (2020), https://doi.org/10.1007/s42452-020-03597-y.
[10] N. Rajamanickam, S. Kumari, V. K. Vendra, B. W. Lavery, J. Spurgeon, T. Druffel, and M.K. Sunkara, Nanotechnology, **27,** 235404 (2016), https://doi.org/10.1088/0957-4484/27/23/235404.
[11] K.G. Lim, H.B. Kim, J. Jeong, H. Kim, J.Y. Kim, and T.W. Lee, Advanced Materials, **26,** 6461–6466 (2014), https://doi.org/10.1002/adma.201401775.
[12] D. Wang, M. Wright, N.K. Elumalai, and A. Uddin, Solar Energy Materials and Solar Cells, **147,** 255–275 (2016), https://doi.org/10.1016/j.solmat.2015.12.025.
[13] L. Etgar, P. Gao, Z. Xue, Q. Peng, A.K. Chandiran, B. Liu, M.K. Nazeeruddin, and M. Gratzel, Journal of the American Chemical Society, **134**, 17396-17399 (2012), https://doi.org/10.1021/ja307789s.
[14] Z. Li, S.A. Kulkarni, P.P. Boix, E. Shi, A. Cao, K. Fu, S.K. Batabyal, J. Zhang, Q. Xiong, L.H. Wong, N. Mathews, and S.G. Mhaisalkar, ACS nano, **8,** 7, 6797-6804 (2014), https://doi.org/10.1021/nn501096h.
[15] X. Zhang, Y. Zhou, Y. Li, J. Sun, X. Lu, X. Gao, J. Gao, L. Shui, S. Wu, and J-M. Liu, Journal of materials chemistry C, **7**, 3852-3861 (2019), https://doi.org/10.1039/C9TC00374F.
[16] L. Lin, L. Jiang, Y. Qiu, and Y. Yu, Superlattices and Microstructures, **104**, 167-177 (2017), https://doi.org/10.1016/j.spmi.2017.02.028.
[17] T. Wang, J. Chen, G. Wu, and M. Li, Science China Materials, **59**(9), 703-709 (2016), https://doi.org/10.1007/s40843-016-5108-4.
[18] Haynes, W (Ed), *CRC handbook of chemistry and physics*, 97th ed. (CRC press, New York, 2017).
[19] S.Z. Haider, H. Anwar, and M. Wang, Semicond. Sci. Technol. **33**(3), 035001 (2018), https://doi.org/10.1088/1361-6641/aaa596.
[20] R Wei, M.Sc Degree Thesis, Queensland University of Technology, 2018.
[21] U. Mandadapu, S.V. Vedanayakam, and K. Thyagarajan, Indian Journal of Science Technology, **10**(11), 1-8 (2017), https://www.researchgate.net/profile/Victor-Vedanayakam-2/publication/316484058_Simulation_and_Analysis_of_Lead_based_Perovskite_Solar_Cell_using_SCAPS-1D/links/5a8afb1caca272017e639098/Simulation-and-Analysis-of-Lead-based-Perovskite-Solar-Cell-using-SCAPS-1D.pdf.

[22] M. Amalina, and M. Rusop, World Journal of Engineering, **9,** 251-256 (2012), https://doi.org/10.1260/1708-5284.9.3.251.
[23] D. Eli, M. Y. Onimisi, S. Garba, R. U. Ugbe, J. A. Owolabi, O. O. Ige, G. J. Ibeh, and A. O. Muhammed, Journal of the Nigerian Society of Physical Sciences, **1**, 72-81, (2019), https://doi.org/10.46481/jnsps.2019.13.
[24] M. I. Hossain, F. H. Alharbi, and N. Tabet, Solar Energy, **120**, 370-380 (2015), https://doi.org/10.1016/j.solener.2015.07.040.
[25] L, Lin, L, Jiang, Y, Qiu, and Y. Yu, Superlattices and Microstructures, **104**, 167-177 (2017), https://doi.org/10.1016/j.spmi.2017.02.028.
[26] P. Gao, M. Gratzel, and M. K. Nazeeruddin, Energy and Environmental Science, **7,** 2448-2463 (2014), https://doi.org/10.1039/C4EE00942H.
[27] U. Mandadapu, S.V. Vedanayakam, and K. Thyagarajan, Int. J. Eng. Sci. Invention, **2**,40-45 (2017).
[28] W. Liu, and Y. Zhang, Journal of materials chemistry A, **2**, 10244-10249 (2014), https://doi.org/10.1039/C4TA01219D.

ЧИСЛЕННЕ МОДЕЛЮВАННЯ ТА АНАЛІЗ ГЕТЕРОПЕРЕХІДНОГО СОНЯЧНОГО ЕЛЕМЕНТА БЕЗ HTM З ВИКОРИСТАННЯМ ПРОГРАМИ SCAPS-1D

Елі Данладі[a], Алхассан Шуайбу[b], Мухаммед Сані Ахмад[b], Джаміла Тасіу[b]
[a]Факультет фізичних наук, Університет Грінфілд, Кадуна, Нігерія
[b]Фізичний факультет, Державний університет Кадуни, Кадуна, Нігерія

У цій дослідницькій роботі пропонується структура перовскітного сонячного елемента (PSC), що не містить HTM (дірково-транспортувальний матеріал), з титаном (TiO_2), метил-амонієвим трийодидом свинцю ($CH_3NH_3PbI_3$) і платиною (Pt) в якості електронно-транспортного матеріалу (ETM), збирача фотонів та металевого зворотного контакту. Для реалізації моделі та моделювання була використана програма «Імітатор Ємності Сонячних Елементів» (SCAPS-1D). Проводилось системне дослідження впливу таких параметрів як товщина ETM, товщина поглинача, концентрація легуючих речовин ETM та поглинача, а також спорідненість до електронів (EA) електронно-транспортного матеріалу (ETM). З отриманих результатів було встановлено, що ці параметри впливають на продуктивність сонячного елемента. Коли товщина ETM змінювалась від 0,02 до 0,10 μm , результати показали, що фотоелектричні параметри зменшуються із збільшенням товщини. Коли товщина поглинача змінювалася від 0,1 до 1,0 μm , оптимізоване значення було встановлено при товщині 0,4 μm . Коли концентрація легуючих речовин поглинача та EMT змінювалась від 10^{10}–10^{17} $см^{-3}$ та від 10^{15}–10^{20} $см^{-3}$, найвищі значення PCE (ефективність перетворення потужності) були отримані при 10^{16} $см^{-3}$ та 10^{20} $см^{-3}$ для поглинача та ETM. Також, коли EA (спорідненість до електронів) змінювалась в діапазоні від 3,7 до 4,5 еВ, оптимізоване значення було на рівні 3,7 еВ. Після оптимізації вищезазначених параметрів було встановлено, що ефективність перетворення потужності (PCE) становить: 25,75%,25,75%, щільність струму короткого замикання (J_{sc}) – 23,25 $мАсм^{-2}$, напруга розімкнутого контуру (V_{oc}) – 1,24 В, і коефіцієнт заповнення (FF) – 89,50%. Оптимізований результат показує підвищення PCE в ~ 1,95 разів, J_{sc} в ~ 1,06 разів, V_{oc} в ~ 1,44 рази і FF в ~ 1,28 разів порівняно з початковим пристроєм із наступними параметрами, PCE = 13,22%, J_{sc} = 21,96 $мАсм^{-2}$, V_{oc} = 0,86 В і FF = 69,94%.

КЛЮЧОВІ СЛОВА: перовскітний сонячний елемент, без HTM (дірково-транспортувальний матеріал), моделювання пристроїв, імітація, зміщення забороненої зони